Deep-Sea Research Part I xxx (xxxx) xxx–xxx

Contents lists available at ScienceDirect

Deep-Sea Research Part I

journal homepage: www.elsevier.com/locate/dsri

CCE V: Primary production, mesozooplankton grazing, and the biological pump in the California Current Ecosystem: Variability and response to El Niño

Rebecca M. Morrow[a], Mark D. Ohman[b], Ralf Goericke[b], Thomas B. Kelly[a], Brandon M. Stephens[b], Michael R. Stukel[a,c,*]

[a] Dept. of Earth, Ocean, and Atmospheric Science, Florida State University, Tallahassee, FL 32308, United States
[b] Scripps Institution of Oceanography, University of California San Diego, San Diego, CA 92093, United States
[c] Center for Ocean-Atmospheric Prediction Studies, Florida State University, Tallahassee, FL 32308, United States

ARTICLE INFO

Keywords:
Carbon export
Fecal pellets
Sinking particles
Interannual variability
Net primary productivity
Eastern boundary upwelling system

ABSTRACT

Predicting marine carbon sequestration in a changing climate requires mechanistic understanding of the processes controlling sinking particle flux under different climatic conditions. The recent occurrence of a warm anomaly (2014–2015) followed by an El Niño (2015–2016) in the southern sector of the California Current System presented an opportunity to analyze changes in the biological carbon pump in response to altered climate forcing. We compare primary production, mesozooplankton grazing, and carbon export from the euphotic zone during quasi-Lagrangian experiments conducted in contrasting conditions: two cruises during warm years - one during the warm anomaly in 2014 and one toward the end of El Niño 2016 – and three cruises during El Niño-neutral years. Results showed no substantial differences in the relationships between vertical carbon export and its presumed drivers (primary production, mesozooplankton grazing) between warm and neutral years. Mesozooplankton fecal pellet enumeration and phaeopigment measurements both showed that fecal pellets were the dominant contributor to export in productive upwelling regions. In more oligotrophic regions, fluxes were dominated by amorphous marine snow with negligible pigment content. We found no evidence for a significant shift in the relationship between mesozooplankton grazing rate and chlorophyll concentration. However, mass-specific grazing rates were lower at low-to-moderate chlorophyll concentrations during warm years relative to neutral years. We also detected a significant difference in the relationship between phytoplankton primary production and photosynthetically active radiation between years: at similar irradiance and nutrient concentrations, productivity decreased during the warm events. Whether these changes resulted from species composition changes remains to be determined. Overall, our results suggest that the processes driving export remain similar during different climate conditions, but that species compositional changes or other structural changes require further attention.

1. Introduction

The biological carbon pump (BCP) refers to a suite of biological, chemical, and physical processes starting with organic matter production by phytoplankton and resulting in transport of this organic matter out of the surface ocean-atmosphere system (Ducklow et al., 2001). The BCP is responsible for the uptake of 5–13 Pg C yr^{-1} (Dunne et al., 2005; Henson et al., 2011; Laws et al., 2011; Siegel et al., 2014), but the processes responsible for this transport remain poorly quantified. Vertical flux of organic matter can be driven by active transport mediated by vertically-migrating organisms, passive transport of particulate and dissolved organic matter during subduction or vertical mixing, or the gravitational settling of phytodetritus, larger organic aggregates, and fecal pellets of zooplankton and fish. Prediction of future changes in the magnitude of the BCP requires understanding the complex processes responsible for particle creation and transformation. The role of herbivorous zooplankton (protists, crustaceans, and gelatinous taxa) may be particularly important due to their roles in controlling primary production and autotroph biomass and in producing rapidly-sinking fecal pellets (Steinberg and Landry, 2017; Turner, 2015; Wilson et al.,

* Correspondence to: Earth, Ocean, and Atmospheric Science Dept., Florida State University, 117N Woodward Ave., OSB 323, Tallahassee, FL 32306-4520, United States.
E-mail address: mstukel@fsu.edu (M.R. Stukel).

https://doi.org/10.1016/j.dsr.2018.07.012
Received 16 January 2018; Received in revised form 19 June 2018; Accepted 18 July 2018

2008).

The southern California Current Ecosystem (CCE) is a spatially heterogeneous environment with high productivity in the coastal upwelling zone, a transition region driven by wind-stress curl upwelling and lateral inputs from the coastal region, and a more-stratified oligotrophic offshore region dominated by picoautotrophs and the microbial loop (Kahru et al., 2015; Venrick, 2002). Previous results from El Niño-neutral years have suggested an important role for mesozooplankton in vertical flux in the CCE. The variability and magnitude of carbon flux from the euphotic zone was consistent with predicted fecal pellet production rates (Stukel et al., 2011). Mesozooplankton fecal pellets were also the dominant recognizable component of sinking material, although in oligotrophic regions most material was unrecognizable marine snow (Stukel et al., 2013). Nevertheless, the generalizability of previous results (derived from three cruises in El Niño-neutral years) to conditions of strong warm anomalies remains in question, as does the responsiveness of mesozooplankton-mediated export to a changing climate.

El Niño-Southern Oscillation (ENSO) is an important driver of ecological variability in the CCE (Rebstock, 2003). El Niño physical impacts on the CCE usually include poleward propagation of tropical waters into the CCE, reduced upwelling favorable winds, and a deepening of the nitracline that together result in decreased nutrient input to surface waters (Alexander et al., 2002; Bograd and Lynn, 2001; Chavez et al., 2002; Frischknecht et al., 2015). This can lead to a compression of the productive coastal region (Kahru and Mitchell, 2000, 2002) and a likely decrease in the cross-shore lateral transport that would support the BCP in transition regions. These drivers can also result in decreased phytoplankton and zooplankton biomass (Chavez et al., 2002; Chelton et al., 1982; Kahru and Mitchell, 2000) and a shift in dominant zooplankton taxa (Fisher et al., 2015; Lavaniegos and Ohman, 2007; Rebstock, 2001).

Despite these predictable El Niño-driven shifts, questions remain about the mechanistic links between physical drivers and ecological and biogeochemical impacts (Clarke and Dottori, 2008; Goericke and Ohman, 2015; Ohman et al., 2013). Are sustained anomalies in advective transport responsible for the observed taxonomic differences? Does altered community composition drive changes in biogeochemical response or is the system-wide outcome simply a linear response to altered upwelling and nutrient inputs? Prior studies addressing the impact of ENSO on the biological pump in the CCE have been restricted to deep-sea moored traps and have shown contrasting results in nearshore and offshore regions (Shipe et al., 2002; Smith et al., 2006).

Our study specifically addresses whether plankton communities and the biological pump respond similarly to equivalent physical and biogeochemical forcing (e.g., nutrient concentrations) irrespective of the climatic conditions. Can intra-regional variability within an ecosystem be utilized to understand inter-annual variability, referred to as a space-for-time exchange? The anomalous physical conditions encountered in the CCE from 2014 to 2016 allows us to directly assess this question. The anomalous conditions began with warming experienced across much of the Northeast Pacific basin beginning in late 2013 and 2014 (Bond et al., 2015; Di Lorenzo and Mantua, 2016; Wang et al., 2014). While the causes of this warming are still being debated, the physical consequences were clear with a substantially deepened nitracline, increased density stratification, and high sea surface temperature anomalies in our study region (Gentemann et al., 2017; Rudnick et al., 2017; Zaba and Rudnick, 2016). Subsurface fields in our study region and along-shore wind patterns suggest that the 2016 warming signal represented the imprint of a significant El Niño on the previous 2014–2015 warming anomaly (Frischknecht et al., 2017; Jacox et al., 2016). Regardless of the physical mechanism, conditions experienced from 2014 to 2016 represented a stark departure from the long-term mean conditions in the CCE, with depressed thermocline and nitracline, increased surface temperatures, and strong stratification (McClatchie et al., 2016).

Here, we utilize a suite of physical, biological, and biogeochemical measurements made on the P1408 and P1604 cruises of the CCE Long-Term Ecological Research (LTER) program that occurred during the anomalously warm periods associated with the northeast Pacific marine heat wave of 2014–2015 and the 2015–2016 El Niño (Bond et al., 2015; Jacox et al., 2016). Quasi-Lagrangian experimental designs and observational measurements made on these cruises are directly comparable to similar measurements made in this region during El Niño-neutral years (Stukel et al., 2011, 2012, 2013). We ask if documented shifts in phytoplankton and zooplankton taxonomic diversity during the warm anomaly and El Niño altered the fundamental underlying relationships between phytoplankton production, zooplankton grazing, and carbon flux. We do not suggest that the magnitude of the BCP is unchanged by such warm conditions (indeed, results from south of our study region show depression of the BCP during El Niño conditions, Silverberg et al., 2004). Rather, we test whether or not the functional response of the BCP to changes in primary production and mesozooplankton activity is unchanged during such warm and El Niño-neutral periods.

2. Methods

2.1. Experimental design

Results are derived from five research cruises of the CCE-LTER program with similar experimental designs and sampling regions (ranging from the Point Conception upwelling center to oligotrophic regions up to 500 km offshore): P0605 in May 2006, P0704 in April 2007, P0810 in October 2008, P1408 in August 2014, and P1604 in April 2016 (Fig. 1). During each cruise, sampling plans were designed around four to six quasi-Lagrangian experiments of 2–5 day duration (hereafter referred to as “cycles”). During these cycles, homogeneous water parcels were identified using a Moving Vessel Profiler (Ohman et al., 2012) and tagged with an experimental array (Landry et al., 2009). Quasi-Lagrangian sampling allowed us to conduct comprehensive ecosystem measurements of water parcels chosen to be representative of the coastal upwelling, transition region, and offshore, more-stratified oligotrophic regions on each cruise. The experimental array consisted of a Globalstar-equipped surface float, a 3-m long × 1-m diameter holey sock drogue centered at 15-m depth, and a coated wire with attachment points for incubating experimental bottles in situ at depths to 110 m. This experimental array served as a moving frame of reference for vertically-resolved sampling of nutrient concentrations, phyto- and zooplankton biomass, phytoplankton production, zooplankton grazing, vertical carbon flux, and computation of net rates of community change in a Lagrangian framework (Landry et al., 2012, 2009). Ecosystem conditions for El Niño-neutral (“neutral year”) cruises were summarized in Stukel et al. (2015). Results from P1408 and P1604 (“warm year”) cruises are first reported here or in other manuscripts in this issue.

2.2. Phytoplankton measurements

Chlorophyll *a* (Chl) and phaeopigment (Phaeo) concentrations were measured at 8 depths spanning the euphotic zone using the acidification method (Strickland and Parsons, 1972). Samples of known volume were filtered through Whatman GF/F filters, extracted in 90% acetone at − 20 °C for 24 h, and quantified on a Turner 10-AU fluorometer. Additional samples for size-fractionated Chl were collected from the near surface layer (all cycles) and deep chlorophyll maximum (some cycles in stratified regions) and filtered through GF/F, 1-μm, 3-μm, 8-μm, and 20-μm filters. The acidification method can be a biased estimator of Phaeo concentrations when Chl *b* is present (Welschmeyer, 1994). Since Chl *b* often comprised 10% of the total chlorophyll in our samples (Goericke, unpublished) our Phaeo measurements should be considered semi-quantitative measurements that are useful for

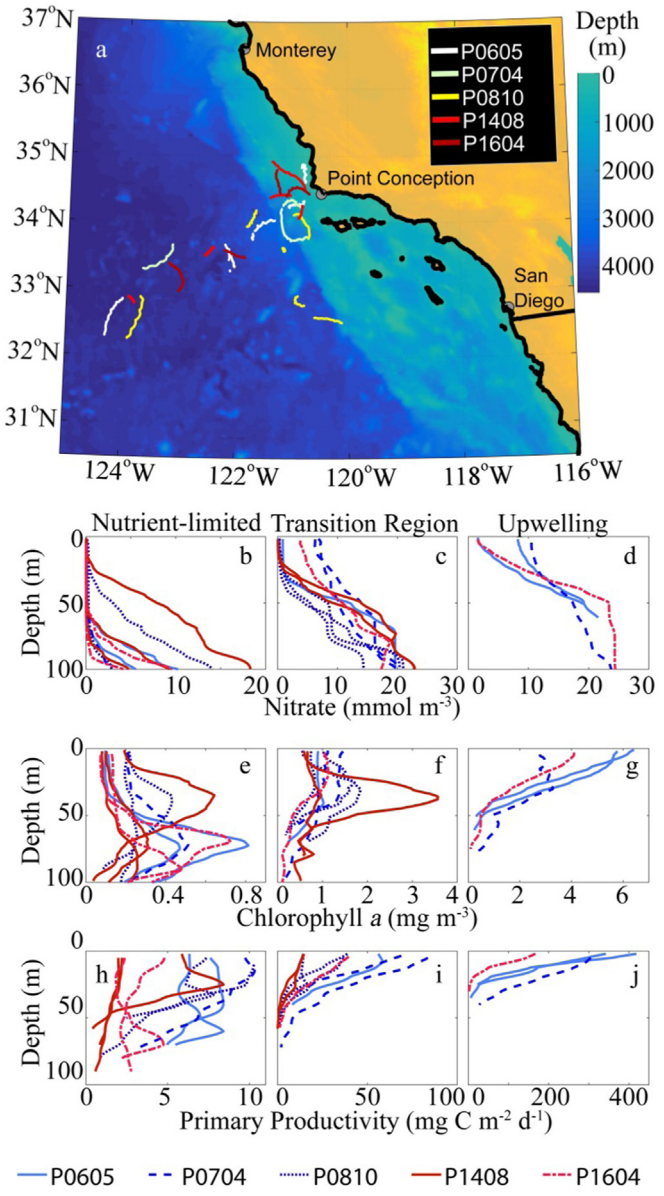

Fig. 1. Experimental cycle characteristics – Study region with Lagrangian cycle drifter locations shown (a) and vertical profiles of nitrate (b, c, d), Chl (e, f, g), and ^{14}CPP (h, i, j) for cycles conducted in water parcels characterized as nutrient-limited (b, e, h), transition region (c, f, i), or coastal upwelling (d, g, j). Vertical profiles are 5-m exponential moving averages of multiple casts per cycle. Note different x-axes in each panel.

assessing relative ratios of Chl:Phaeo in water column and sediment trap samples, but are not ideal for quantification of total Phaeo standing stock.

Primary production (^{14}C-PP) was measured by $H^{14}CO_3$ uptake daily at 6–8 depths spanning the euphotic zone. Incubations began pre-dawn and lasted 24 h. From 2006 to 2008 samples were measured in 4-L polycarbonate bottles that were incubated in situ on the experimental array and subsampled in triplicate post-incubation. From 2014 to 2016 samples were measured in triplicate 250-mL bottles similarly incubated in situ. Separate 250-mL dark bottles were used as blanks on each cruise to correct for adsorption or non-photosynthetic ^{14}C uptake. After incubation, samples were filtered through a GF/F filter, placed in scintillation cocktail, and counted on a liquid scintillation counter.

Surface photosynthetically active radiation (PAR) was measured using a 2-π Licor PAR sensor. Photosynthetically active radiation (PAR) in the water column was measured using a 4-π Licor PAR sensor mounted on a CTD rosette. The % surface irradiance at our sampling depths was calculated from *in situ* PAR and surface PAR. Daily average PAR at sampling depths was calculated from surface PAR integrated over the day and % surface irradiance.

2.3. Zooplankton measurements

Mesozooplankton were collected twice daily (late morning and near midnight) via oblique bongo net tows (target depth of 210 m, 0.71-m diameter net, 202-μm mesh). One bongo sample was preserved for taxonomic analysis and the other utilized for biomass and gut pigment measurements. The latter sample was immediately anesthetized with carbonated water, split on a Folsom splitter, and size-fractionated through nested meshes (0.2–0.5 mm, 0.5–1.0 mm, 1–2 mm, 2–5 mm, > 5 mm). Biomass samples were rinsed with isotonic ammonium formate onto pre-tared filters. Samples were then flash frozen in liquid nitrogen for analysis ashore.

Gut pigment samples were examined on ice under a stereo microscope to remove phytodetritus. Mesozooplankton were then transferred into 90% acetone in an ice bath, sonicated with an ultrasonic probe, and allowed to extract at − 20 °C for 24 h. Samples were then centrifuged and analyzed for Chl and Phaeo by the acidification method. Grazing rate was determined from the sum of Chl and Phaeo using the updated temperature-dependent gut turnover rate (k) of Dam and Peterson (1988) as reported in Bamstedt et al. (2000): k (min^{-1}) = $0.0124 \times e^{0.07675T}$. T was the temperature at the depth of the Chl maximum. Dry mass was determined by drying samples at 60 °C for 24 h, then weighing on a microbalance.

2.4. Carbon export measurements

VERTEX-style particle interceptor traps (PIT, Knauer et al., 1979) were deployed on P0704, P0810, P1408, and P1604 on a separate drifting array similar to the incubation array. The sediment trap array supported crosspieces with 8–12 PIT tubes with a 70-mm inner diameter, an 8:1 aspect ratio (height:diameter), and a baffle on top consisting of 13 acrylic tubes with a similar 8:1 aspect ratio and tapered ends. Tubes were deployed with a poisoned hypersaline solution made from 0.1-μm filtered sea water amended with 50 g L^{-1} NaCl and 0.4% (final concentration) formaldehyde. On all cruises, sediment trap crosspieces were deployed at a depth of 100 m. On P0810 and warm year cruises, traps were deployed at 100-m and at a depth slightly below the base of the euphotic zone (estimated before deployment from fluorescence profiles) if the euphotic depth was shallower than 80-m. These euphotic zone traps were at a depth of 50 m on 0810-1, 0810-4, and 1604-4; 60 m on 0810-3, 0810-5, 0810-6, 1408-1, 1408-2, 1408-3, and 1604-3; and 70 m on 1408-4. All trap deployments were at depths substantially deeper than the depth of the mixed layer. On warm year cruises an additional trap array was placed at 150-m depth. Due to a shark bite and subsequent re-splicing of the sediment trap array line, depths for cycles 1604-2, 1604-3, and 1604-4 were three meters shallower than normal (97 and 147 m). We group these with 100 and 150 m depth samples from other cycles, because remineralization over 3 m is negligible.

After recovery, ambient water that had mixed into the upper layer of the tubes was removed by gentle suction. Samples were then homogenized by slow inversion and 50-mL samples were removed for Chl and Phaeo analyses (analyzed as above for water column samples). Samples were then further split using a Folsom splitter to generate samples for organic C and N, ^{234}Th, and microscopic analysis of sediment trap contents. Samples for C/N were filtered through pre-combusted GF/F filters and frozen at − 80 °C, then acidified to remove inorganic carbon and analyzed by either an elemental analyzer or an isotope ratio mass spectrometer at the Scripps Institution of Oceanography. Samples for ^{234}Th were filtered onto pre-combusted quartz (QMA) filters and analyzed on a RISO beta counter (as explained

below). Samples for microscopic analysis were stored at room temperature prior to analysis. They were then placed in a settling chamber and the liquid was poured through a 60-μm filter to capture any fecal pellets that had not sunk to the bottom of the chamber. Samples were transferred to a gridded petri dish and random grids were analyzed under a stereomicroscope (Zeiss Discovery V12 for most years and Zeiss Discovery V20 for P1604). Fecal pellets were not enumerated on the P1408 cruise. Pellets were categorized into 6 shape categories (ovoid, cylindrical, spherical, tabular, amorphous, and ellipsoid) and length/width were determined by image analysis in Image Pro (most years) or Image J (P1604). Pellet volume was determined from length and width using appropriate equations for each shape. Volume was converted to fecal pellet carbon from mean carbon: volume relationships determined for the CCE (0.125 mg C mm^{-3} for ovoid, spherical and ellipsoid pellets, 0.055 mg C mm^{-3} for cylindrical and amorphous pellets, and 0.029 mg C mm^{-3} for tabular pellets, Stukel et al., 2013).

Samples for water column total ^{234}Th were analyzed using standard small-volume techniques (Benitez-Nelson et al., 2001; Pike et al., 2005). Briefly, 4-L samples were taken from a Niskin bottle, immediately acidified to a pH < 2 with HNO_3, and spiked with 1-mL of ^{230}Th tracer. After > 4 h, samples were brought to a pH of 8–9 with NH_4OH, and $MnCl_2$ and $KMnO_4$ were added. Samples were shaken vigorously and allowed to sit for > 8 h, then filtered onto QMA filters. Filters were mounted into RISO sample holders and counted on a RISO beta counter (at sea for P1408 and P1604 cruises and at the University of South Carolina after P0605, P0704, and P0810 as presented in Stukel et al. (2011, 2013)). More than 6 months later background counts were determined and samples were dissolved in 8 M HNO_3/10% H_2O_2, spiked with ^{229}Th tracer, and purified by column chromatography with AG1-X8 resin. Samples were then analyzed by inductively-coupled plasma mass spectrometry at the Woods Hole Analytical Facility (P0605, P0704, P0810) or the National High Magnetic Field Laboratory (P1408, P1604) to determine the $^{229:230}$Th ratio and calculate the yield of ^{234}Th during the initial filtration step. ^{238}U-^{234}Th deficiency was calculated by estimating ^{238}U from salinity using the relationship of Owens et al. (2011). ^{234}Th flux was calculated using a simple 1-D steady state model.

2.5. Statistical analyses

Unless otherwise stated, error bars shown in graphs are the standard error of replicated measurements. Type II linear regressions with uncertainty in both variables were calculated according to York et al. (2004). Uncertainty analysis on all functional relationships (e.g., linear regressions, photosynthesis-irradiance curves, or grazing-Chl relationships) was conducted using non-parametric boot-strapping techniques (random sampling with replacement), because data were not normally distributed. With relationships for which > 50 measurements were available (e.g., photosynthesis-irradiance) we conducted a standard bootstrap with > 1000 bootstrap samples. Functions were fit using a grid search approach that minimized root mean squared error. For relationships with < 50 measurements (e.g., grazing-Chl) we utilized a modified bootstrapping approach. First, a simulated dataset was created from the mean and standard deviation of each data point. Then a random sample was drawn from this simulated dataset as in standard bootstrapping. This procedure was iterated to generate > 1000 bootstrap samples. This approach thus accounts for variable measurement uncertainty. The 95% confidence intervals (95% C.I.) on relationships are plotted. Since our goal was to determine whether the functional relationship was different between warm and neutral year cruises (rather than to determine the shape of the functional relationship) we typically assumed a specific shape for the relationship (e.g., Ivlev for grazing) based on *a priori* knowledge and tested for variability in the parameters between cruises. Our chosen functional forms do not imply that these are the only (or most appropriate) functional forms that could explain relationships in the data.

3. Results

3.1. Description of water parcels

By design, each cruise sampled a range of water parcels spanning substantial ecosystem variability (Fig. 1). Across the five cruises, surface Chl concentrations ranged from 0.07 μg Chl L^{-1} (cycle 1604-4) to 6.6 μg Chl L^{-1} (cycle 0605-3). Within individual cruises, the range of variability in surface Chl was 0.10–6.6 μg Chl L^{-1} for P0605, 0.21–2.4 μg Chl L^{-1} for P0704, 0.21–1.4 μg Chl L^{-1} for P0810, 0.08–0.66 μg Chl L^{-1} for P1408, and 0.07–4.2 μg Chl L^{-1} for P1604 (Fig. 1e-g). Surface NO_3^- showed similarly high variability with minimum values near the detection limits on all cruises and maximum values exceeding 4 μmol NO_3^- L^{-1} on all cruises except P1408 (Fig. 1b-d). The relatively low variability encountered on the P1408 cruise reflected a region-wide warming anomaly that compressed the natural spatial variability across the CCE. During the P1604 cruise, which occurred toward the end of the 2015–2016 El Niño, the productive region was compressed along the coast, but nevertheless sampled during cycles 1604-3 and 1604-4.

Based on distance from shore and nutrient, temperature, Chl, and ^{14}CPP profiles, we classified the water parcels studied into three broad classes: Coastal upwelling water parcels had high surface Chl (> 2.5 mg m^{-3}) and nitrate concentrations (> 1.5 mmol m^{-3}) and high surface ^{14}CPP (> 160 mg C m^{-2} d^{-1}). Transition region water parcels had low to moderate surface nitrate (0.06–7 mmol m^{-3}), moderate surface Chl and ^{14}CPP (0.5–1.5 mg m^{-3}, and 14–84 mg C m^{-2} d^{-1}, respectively), and relatively shallow nitracline depths. Nutrient-limited water parcels had low surface nitrate and Chl (< 0.3 mmol m^{-3} and < 0.25 mg m^{-3}, respectively), a deep nitracline, and a deep Chl maximum. Based on these characterizations, we sampled 10 water parcels that could be characterized as nutrient-limited (0605-2, 0605-5, 0704-2, 0810-2, 0810-6, 1408-3, 1408-4, 1408-5, 1604-1, and 1604-2), 10 water parcels that could be characterized as transition region (0605-4, 0704-1, 0704-4, 0810-1, 0810-3, 0810-4, 0810-5, 1408-1, 1408-2, and 1604-3), and 3 water parcels that could be characterized as coastal upwelling (0605-1, 0605-3, and 1604-4; however we have no carbon export measurements from 0605-1 or 0605-3). We thus successfully sampled a broad range of conditions during both neutral and warm years, but did not sample any coastal upwelling communities during fall cruises (P0810 and P1408). This is not surprising, as upwelling favorable winds in the CCE are most common in the spring and summer.

3.2. Response of primary productivity to nutrients and light

Bulk primary production is dependent on the functional responses of each taxon in the diverse phytoplankton community to *in situ* photosynthetically active radiation (PAR), the color spectrum of PAR, the availability of macro- and micronutrients, and the physiological status of the cells. Nevertheless, broad spatiotemporal patterns in primary productivity can be predicted from ambient NO_3^- and PAR. In both warm and neutral years, a clear pattern emerges of low primary production (typically < 3 μg C L^{-1} d^{-1}) in low NO_3^- water (< 0.2 μmol L^{-1}). At higher NO_3^- concentrations primary production is a strong function of PAR and ranges from < 0.1 μg C L^{-1} d^{-1} at low irradiance to > 100 μg C L^{-1} d^{-1} when light is saturating (Fig. 2a,c). When normalized to Chl to estimate phytoplankton specific production (though we note that due to variable C:Chl this is not the same as biomass-normalized specific production) primary production showed a strong relationship with light, but no statistically significant response to NO_3^- (Fig. 2b). This implies that nutrient concentration sets the biomass of the euphotic zone community, while PAR is an important control on phytoplankton specific growth rates.

To quantitatively compare the growth responses of phytoplankton between warm and neutral years, we fit the specific production rate and PAR data to a function of the form: $PP/chl = V_{0\,m} \times [1\text{-}exp(-\alpha \times PAR/$

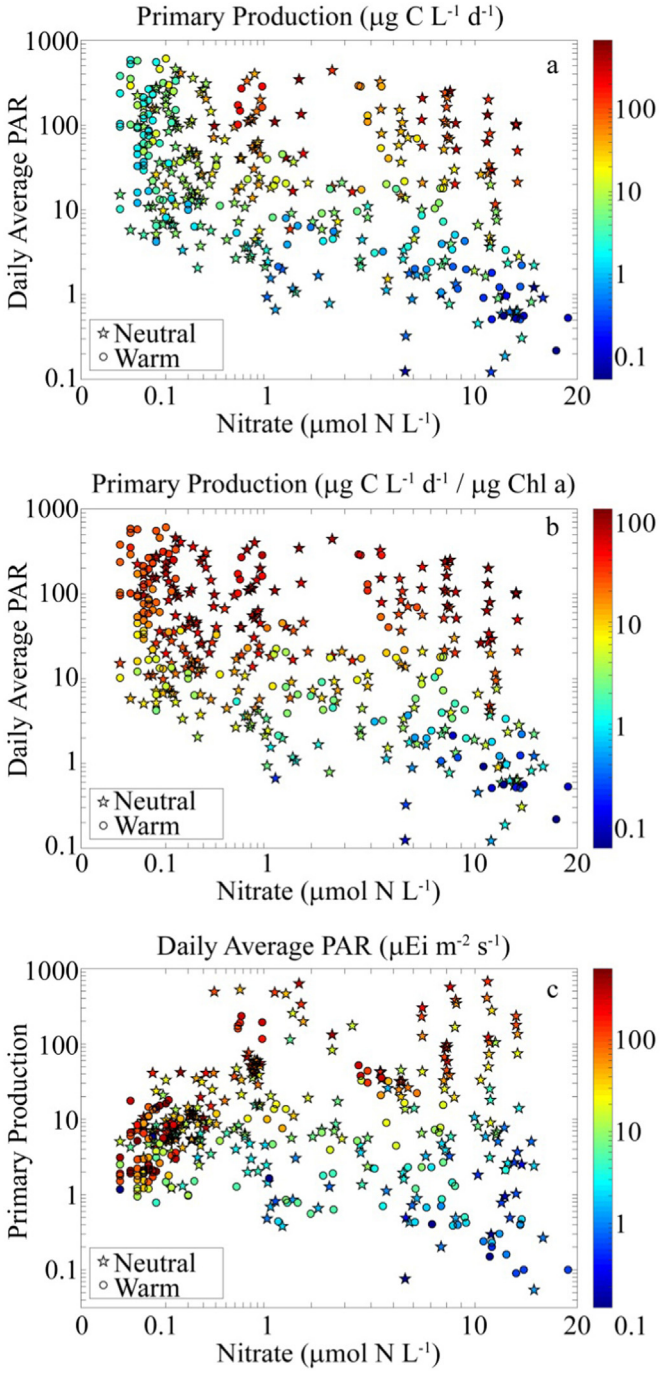

Fig. 2. Primary Production Response to El Niño – a) Primary production as a function of nitrate and photosynthetically active radiation (PAR, µEi m^{-2} s^{-1}). b) Specific primary production (PP normalized to Chl *a*) as a function of nitrate and PAR. c) Nitrate vs primary production (µg C L^{-1} d^{-1}) with PAR on the color axis. In (a), (b), and (c) stars are "neutral" years (2006–2008) and circles are "warm" years (2014 and 2016). (For interpretation of the references to color in this figure legend, the reader is referred to the web version of this article.)

V_{0m})] × exp(-β × PAR/$V_{0\,m}$). This relationship is widely used in biogeochemical models and production-irradiance (PI) studies and assumes that phytoplankton show an initial rapid increase with PAR, before becoming light saturated and eventually photo-inhibited. $V_{0\,m}$ is the Chl-specific maximum growth rate of the phytoplankton, α is the Chl-specific initial slope of the PI curve, and β is the photoinhibition coefficient. When using all data, we found a best fit with values of $V_{0\,m}$ = 64 mg C d^{-1}/mg Chl, α = 1.0, and β = 0.049 (Fig. 3a). However, we found statistically significant differences (> 95% confidence, determined by non-parametric bootstrapping analysis) between the relationships for warm and neutral years that reflected a roughly 2–3 fold higher chl-specific growth rate for phytoplankton during neutral years relative to warm years at identical PAR. A similar relationship was found when the data were grouped based on oceanic province (nutrient-limited, transition region, or coastal upwelling), with coastal upwelling water parcels exhibiting higher primary productivity per Chl than nutrient-limited water parcels at similar PAR (Fig. 3b). The magnitude of the difference was approximately 50% weaker when comparing coastal upwelling to nutrient-limited data than when comparing neutral to warm years.

3.3. Response of mesozooplankton grazing to Chl a

Zooplankton grazing (and fecal pellet production) rates are fundamentally functions of zooplankton biomass and prey concentration. However, the functional form of the relationship of ingestion to prey concentration will vary based on taxon-specific behavior, particle capture mechanisms, and dietary preferences. Furthermore, the prey available to different taxa are highly variable (e.g., appendicularians can feed on picoplankton that are inaccessible to most crustaceans). Such taxon-specific differences are potentially relevant, because our study included mesozooplankton communities variously dominated by doliolids (1604-3), salps (1408-2), euphausiids (0704-1 and 0704-4), large calanoid copepods (1604-4), and mixed assemblages of small crustaceans (most nutrient-limited cycles). Because we cannot quantify community differences here, we tested the null hypothesis that overall mesozooplankton grazing showed the same response to changes in Chl among years.

There was no consistent difference in the relationship between mesozooplankton biomass (as dry mass) and nanoplankton + microplankton (> 3-µm) Chl averaged across the euphotic zone when comparing neutral with warm years (Fig. 4a). Ingestion rates varied with nanoplankton + microplankton Chl, with a linear regression of log-transformed data showing no significant differences between warm and neutral years (Fig. 4b). Grazing rates at some locations during warm years were low (Fig. 4b), but not unexpected from the lower Chl concentrations. One point on cruise P0704 (Cycle 1) departed markedly from the functional relationship because a dense patch of euphausiids was sampled there. Mass-specific grazing rates (Fig. 4c) show evidence of saturation, as reflected by Ivlev fits. Notably, mass-specific grazing rates in warm years (2014 and 2016) were lower than expected from the relationship developed during El Nino-neutral years (Fig. 4c), although the 95% uncertainty intervals for the two periods overlapped.

3.4. Spatiotemporal variability of export flux

To assess the accuracy of sediment trap measurements, we compared ^{234}Th flux of particles collected in trap tubes to ^{234}Th fluxes estimated from ^{238}U-^{234}Th disequilibrium (Fig. 5). Results showed a good agreement between sediment trap ^{234}Th flux and ^{234}Th flux estimated from water column measurements and a one-dimensional steady-state export model. The median ratio of sediment trap-derived export to steady-state export was 0.98, suggesting that on average our sediment traps estimated 2% lower sinking fluxes than the ^{238}U-^{234}Th disequilibrium method. The deployment with the greatest discrepancy between sediment trap and steady-state model flux was cycle P0810-4 (both depths), which occurred immediately after strong upwelling-favorable winds commenced, likely introducing ^{234}Th-rich water to the surface layer and violating the assumptions of our one-dimensional steady state model (Fig. 5).

Sediment trap-derived carbon flux at 100 m depth (available for P0704, P0810, P1408, and P1604 cruises) showed substantial spatial variability within each cruise (Fig. 6a). Flux was high in the lone coastal

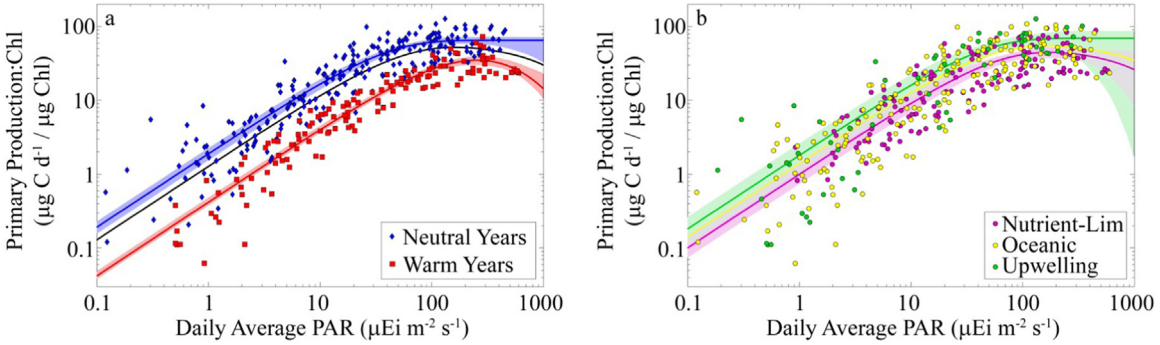

Fig. 3. Functional relationship of phytoplankton production to light. a) Warm vs. neutral years. Functional relationship is: $PP/chl = V_{0m} \times [1\text{-}exp(-\alpha PAR/V_{0m})] \times exp(-\beta PAR/V_{0m})$. Black line shows the relationship for all data, red and blue lines for warm and neutral years, respectively. b) As in (a) except data are grouped by water parcel type (nutrient-limited, transition region, coastal upwelling). Error bounds show 95% confidence intervals for the functional relationship (not for prediction of individual points) as determined by non-parametric bootstrapping uncertainty analysis. Error bounds are not shown for transition region data in (b). (For interpretation of the references to color in this figure legend, the reader is referred to the web version of this article.)

cycle on which we deployed sediment traps (255 ± 55 mg C m^{-2} d^{-1}), intermediate in transition region cycles (mean = 119 mg C m^{-2} d^{-1}, range = 74 – 170), and low in nutrient-limited cycles (mean = 55 mg C m^{-2} d^{-1}, range = 32–107). The P0704 (23–170 mg C m^{-2} d^{-1}), P1408 (38–159 mg C m^{-2} d^{-1}), and P1604 (40–255 mg C m^{-2} d^{-1}) cruises all showed similar ranges in export flux, while the P0810 cruise had relatively lower variability between cycles (69–149 mg C m^{-2} d^{-1}). Although export flux was measured at only a single depth on P0704, all other cruises showed moderate attenuation of flux with depth. Across all cycles with traps deployed at multiple depths, the median of an exponential relationship expressing export flux attenuation with depth suggested a remineralization constant of 7.1×10^{-3} m^{-1}. This suggests a ~ 50% attenuation of carbon flux as sinking particles penetrate 100 m deeper into the ocean.

Regional variability in particle flux was relatively high (intra-cruise fluxes varied by a factor of 2.2–7.4), but it was slightly lower than regional variability in primary production rates (intra-cruise vertically-integrated primary production varied by a factor of 3.2–7.5). This dampened export variability relative to primary production was reflected in the functional relationship of export to primary productivity. A Type II linear regression expressing carbon export in relation to primary production showed a slope of 0.070 (95% C.I. = 0.03–0.21) and an intercept of 33.5 (95% C.I. = 1.3–64.3; Fig. 6b). The positive intercept was statistically significant and suggests that even in regions with negligible primary productivity we should expect measurable particle flux. For both warm and neutral years, export measurements exceeded the value predicted by the regression for roughly half the Lagrangian cycles and were less than the predicted value for the other half. The slope of the regression determined for warm years (0.068) was greater than the slope for cold years (0.032), although neither was statistically significant and the slope for the warm years was strongly determined by the high value for the coastal upwelling water parcel sampled during cycle 1604-4.

3.5. Response of gravitational flux to mesozooplankton dynamics

A Type II regression of carbon export in relation to mesozooplankton grazing showed a statistically significant positive slope (13 mg C exported/mg Chl grazed, 95% C.I. = 4–39) and intercept (32 mg C m^{-2} d^{-1}, 95% C.I. = 10–44; Fig. 6c). This single regression was a reasonable predictor for measurements from both warm and neutral years. However, uncertainty was quite high during high grazing rate periods. Cycle 0704-2, which sampled a dense euphausiid swarm as noted above, showed only moderate export rates. Conversely, Cycle 1604-4, which had the highest grazing rate in the warm years also had the highest export rates measured.

The ratio of Chl:Phaeo measured in the sediment traps provides a measure of the relative contribution of herbivorous fecal pellets and fresh phytoplankton to sinking flux. The median Chl:Phaeo ratio for sinking material across all samples was 0.11 (95% C.I. was 0.06–0.15) and there was no statistically significant difference between warm (median = 0.08, 95% = 0.03–0.16) and neutral (median = 0.11, 95% = 0.07–0.18) years (Fig. 7a). These median values are not dissimilar from Chl:Phaeo ratios measured in copepod fecal pellets (Downs and Lorenzen, 1985), so we cannot rule out the possibility that Chl in the traps was transported primarily within fecal pellets rather than ungrazed sinking phytoplankton. These sediment trap Chl:Phaeo ratios were also substantially lower than Chl:Phaeo ratios of vertically suspended POM in the euphotic zone, which ranged from 1.0 to 3.6 (median = 2.2, Fig. 7b).

A Type II regression of log-transformed Phaeo flux on log-transformed POC flux suggests a power law relationship: Phaeo Flux = 0.11 × (POC Flux)$^{2.0}$ (Fig. 7c). The exponent had a 95% C.I. of 1.7–2.7. A Type II regression of non-transformed Phaeo flux on POC flux had a slope of 19 µg Chl *a* equivalent/mg POC (9.7–32) and a y-intercept of − 510 µg Chl *a* equivalents m^{-2} d^{-1} (− 1500 to − 200). Regardless of which relationship more accurately describes the relationship between pigment flux and total POC flux, fecal pellets derived from recent herbivory comprise a greater proportion of export when POC flux is high and are a negligible component of the sinking material when flux is < 50 mg C m^{-2} d^{-1} (the geometric mean of Phaeo:C flux was 3.8 for all samples with total C flux < 50 mg C m^{-2} d^{-1}; for comparison, the geometric mean of Phaeo:C was 20 for samples with C flux > 150 mg C m^{-2} d^{-1}).

Microscopic enumeration of recognizable fecal pellets in the sediment traps showed similar patterns between warm and neutral years (Fig. 8a). In coastal regions, fecal pellet flux was high and variable (reaching maximum cycle average values at 100 m of 140 mg C m^{-2} d^{-1} on 0704–1 and 235 mg C m^{-2} d^{-1} on 1604–4). For both of these cycles, recognizable fecal pellets comprised > 90% of total C flux (Fig. 7c and d). In oligotrophic regions, fecal pellet flux was substantially lower (often < 20 mg C m^{-2} d^{-1} during oligotrophic cycles on all cruises) as was the relative contribution of recognizable fecal pellets to total flux (typically < 30% on oligotrophic cycles). During both warm and neutral years cylindrical fecal pellets (likely derived from copepods or euphausiids) were consistently the dominant components of fecal pellet flux. Unsurprisingly, Phaeo flux was strongly correlated with the flux of recognizable fecal pellet carbon into the sediment traps (Fig. 8b). A Type II linear regression of log-transformed data returned a slope of 1.0 (95% C.I. = 0.8–1.3), suggesting a linear relationship for the un-transformed data: Fecal Pellet Flux (mg C m^{-2} d^{-1}) = 0.018 × Phaeo Flux (µg Chl *a* equiv. m^{-2} d^{-1}). Although comprehensive fecal pellet analysis was not conducted for the P1408 cruise, we quantified the large salp pellets that were retained on a 200-

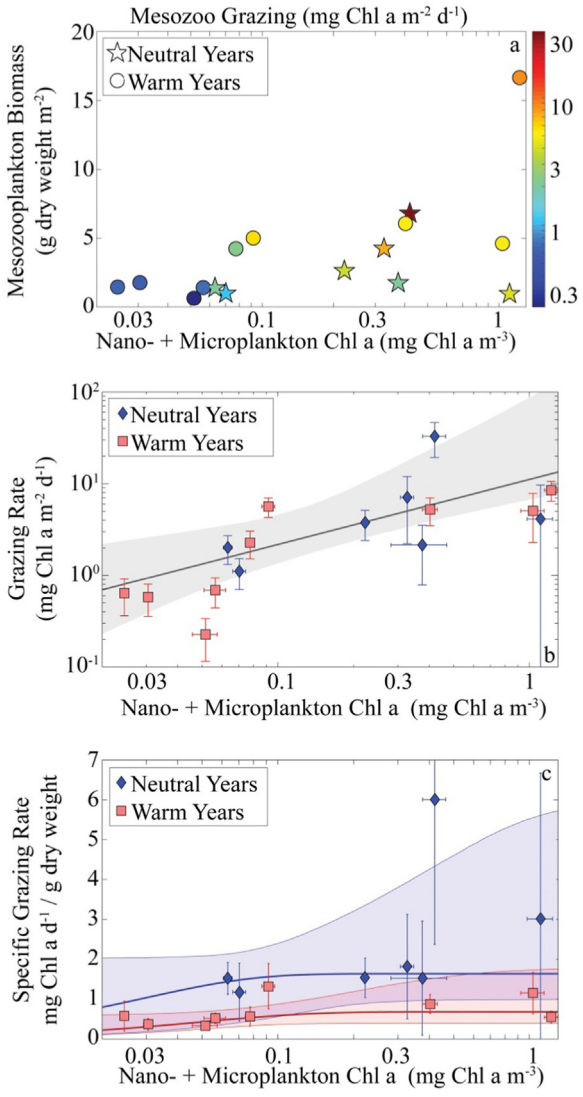

Fig. 4. Mesozooplankton grazing and its relation to nano- and microplankton biomass (average euphotic zone Chl a × fraction Chl a in the > 3-μm size fraction, mg Chl a m^{-3}, x-axis in all panels). a) Mesozooplankton biomass (g dry weight m^{-2}) plotted against nano- + microplankton Chl (mg Chl m^{-3}) with grazing rates (determined by gut pigment methods) shown on the color axis (mg Chl m^{-2} d^{-1}). b) Mesozooplankton bulk grazing rates plotted against nano- + microplankton Chl. Black line is a Type II linear regression: $\log_{10}(\text{Grazing}) = 0.71 \times \log_{10}(\text{Chl}) + 1.0$. c) Mesozooplankton specific grazing rates (mg Chl d^{-1}/g dry weight) plotted against nano- + microplankton Chl. Solid lines are the fits for Ivlev relationships: Specific Grazing $= 1.6 \times 10^{-3} \times (1\text{-exp}(-34 \times \text{Chl}))$ during neutral years and Specific Grazing $= 6.8 \times 10^{-4} \times (1\text{-exp}(-20 \times \text{Chl}))$ during warm years. Uncertainty estimates are standard deviation (σ) of multiple net tows during a cycle. (For interpretation of the references to color in this figure legend, the reader is referred to the web version of this article.)

μm filter. Across all cycles and depths for this cruise (when salp populations were abnormally high, likely because of an intrusion of subtropical water into the region, M. Ohman, unpubl.) fecal pellet flux attributable to large salps was 13 mg C m^{-2} d^{-1} (range = 0–48 mg C m^{-2} d^{-1}).

4. Discussion

4.1. El Niño impacts on carbon export

Physical and biogeochemical conditions experienced from 2014 to 2016 differed substantially from mean conditions in the CCE, with depressed thermocline and nitracline, increased surface temperatures, and strong stratification (McClatchie et al., 2016). Biological consequences of this eastern North Pacific marine heat wave included: decreased phytoplankton biomass coupled with very low mesozooplankton biomass and high protistan grazing rates off Baja California (Gómez-Ocampo et al., 2017; Linacre et al., 2017; McClatchie et al., 2016); altered vertical patterns of ichthyoplankton above the oxygen minimum zone off southern Mexico (Sánchez-Velasco et al., 2017); the appearance of unusual North Pacific gyre copepod taxa in coastal waters off Oregon (Peterson et al., 2017); high abundance of larvaceans and doliolids and a poleward shift in distribution and altered phenology of sardine and anchovy larvae in the northern California Current (Auth et al., 2017; Peterson et al., 2017); and an extensive bloom of the harmful diatom *Pseudo-nitzschia* (McCabe et al., 2016; McKibben et al., 2017). Within our study region, impacts included: substantially decreased Chl concentrations (Kahru et al., in this issue); a decrease in areally-averaged primary production (Kelly et al., in this issue); high concentrations of the pelagic red crab (*Pleuroncodes planipes*) in California coastal waters (McClatchie et al., 2016); an increase in the abundance of subtropical and offshore mesozooplankton taxa (Lilly and Ohman, in this issue); and decreased frequency of sea surface Chl and temperature fronts (Kahru et al., in this issue).

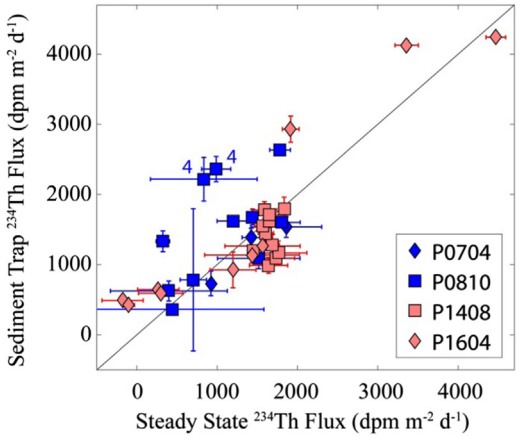

Fig. 5. Sediment trap measured ^{234}Th flux (y-axis) compared to ^{234}Th flux calculated from water column ^{238}U-^{234}Th deficiency measurements and a one-dimensional, steady-state model without upwelling. Black line is the 1:1 line.

Despite these community shifts at multiple trophic levels, we found little evidence for changes of functional relationships between the processes driving the biological pump that could not be explained by bottom-up nutrient regulation of primary production and mesozooplankton grazing. The magnitude and variability of carbon export was similar within comparable water types before and during the oceanic warming event (although the warm event did lead to a decrease in region-wide export as a result of compression of the high productivity region, Kelly et al., in this issue). Furthermore, during both warm and neutral conditions, the recognizable component of sinking material was primarily mesozooplankton fecal material. This material was recognizable as identifiable fecal pellets and phaeopigment tracers, suggesting that recent herbivory was a dominant source for the fecal pellets. Nevertheless, during both climatic periods there was also evidence for additional carbon flux likely regulated by relatively slowly sinking marine snow with no associated pigments.

We found some evidence that during neutral years specific grazing was higher (at a similar Chl concentration) than during warm years. However, the relationships were not significantly different at the 95% level. Furthermore, the decreased specific grazing rates during the warm period seem to have been compensated for by slightly higher mesozooplankton biomass at a similar phytoplankton concentration.

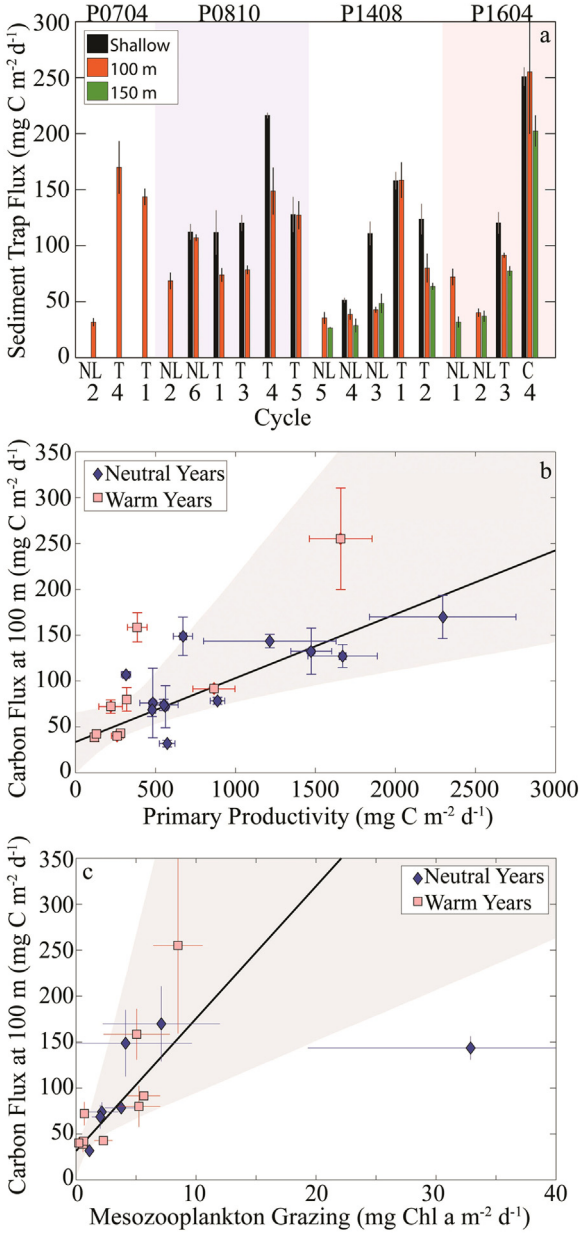

Fig. 6. Export measurements. a) Sediment trap flux measured on each cruise at up to three depths. 'Shallow' traps were placed just below the base of the euphotic zone when the euphotic zone was shallower than 80 m. Within a cruise, cycles are organized in order of increasing surface Chl. Cycles are labeled as nutrient-limited (NL), transition region (T), or coastal upwelling (C). b) Carbon flux as a function of ^{14}C primary productivity. Sediment trap results are plotted for all cruises except P0605 when sediment traps were not deployed and hence ^{234}Th-based carbon export measurements are plotted instead. Black line is a Type II linear regression: Export = 0.070× PP +33.4. c) Carbon flux as a function of mesozooplankton grazing (measured by the gut pigment method). Black line is a Type II linear regression: Export = 14.4 × grazing + 31.5. Gray shaded areas show 95% C.I. on regressions.

Hence the response of community grazing to changing Chl concentrations was largely unchanged by the warming. Similarly, Nickels and Ohman (2018) found that egg production rates of three CCE copepod species were unaffected by the 2014–15 warming event and 2015–16 El Niño. However, our grazing measurements made in a euphausiid-dominated water parcel in April 2007 were a notable outlier from the grazing-Chl relationship (Fig. 4). Euphausiid community composition is substantially altered by El Niño (Lavaniegos and Ohman, 2007; Lilly and Ohman, in this issue; Ohman et al., 2017), suggesting the possibility that their biogeochemical impacts (e.g., on carbon export) may also be affected.

The one statistically significant difference between warm and neutral years was decreased specific primary production during the warming events. ^{14}CPP measurements showed that at similar light levels, primary production was significantly lower during warm years (by a factor of 2–3). This difference could not be explained by differences in contemporaneous nutrient concentrations. It is possible that decreased primary production was caused by decreased abundance of rapidly growing taxa (especially coastal diatom species) as a result of decreased upwelling or advection of subtropical taxa into the region. Previous studies have shown that increased maximum growth rates of diatoms can explain a similar difference in growth-PAR relationships between coastal and oligotrophic regions of the CCE (Li et al., 2010). Nevertheless, it remains unclear why coastal taxa with high growth rates would not have been present in high nutrient water parcels sampled during the warm events. More evidence is needed to determine whether this is a consistent pattern between warm and neutral periods and to ascertain the mechanisms leading to such changes.

4.2. Biological pump responses to ecosystem variability

Prediction of marine carbon sequestration under anthropogenic climate forcing requires a mechanistic understanding of the ecosystem relationships driving the biological carbon pump. Prior research has suggested an important, potentially causal, link between mesozooplankton fecal pellet production and sinking POC in the CCE (Stukel et al., 2011, 2013). If true, we should expect increased export efficiency in coastal regions where production by large diatoms and dinoflagellates is directly available to mesozooplankton grazers (Michaels and Silver, 1988). Indeed, trophic cycling relationships, built upon assumptions about utilization of small and large phytoplankton by different grazer guilds predict that coastal regions should have high export ratios (Siegel et al., 2014; Stukel et al., 2015, 2011). This supposition is not, however, borne out by our data. In fact, if we conduct a Type II linear regression on log-transformed data to determine a power law relationship between export and primary production we find an exponent that is less than one (statistically significant at the 95% C.I.).

A Type II linear regression on log-transformed export and mesozooplankton grazing determined an exponent that was less than one (although this exponent was only less than 1.0 at the 92% C.I.), indicating that export increases more slowly than grazing. This result was, however, strongly driven by the very high grazing rates encountered during the euphausiid swarm on cycle 0704-1. This cycle thus deserves additional attention. The euphotic zone was relatively shallow in this water parcel (1% light level was at ~ 40 m) and primary production was maximal at the surface with moderate primary production (1215 mg C m^{-2} d^{-1}) and export (144 mg C m^{-2} d^{-1}) at 100 m depth (the only depth that sediment traps were deployed during that cruise). However, Jackson and Checkley (2011) used a laser optical plankton counter mounted on an autonomously profiling float to estimate particle flux attenuation with depth during this cycle and found substantial remineralization beneath the euphotic zone. They estimated that flux decreased by a factor of ~ 40 between the particle flux maximum at 30–40 m and our sediment trap at 100 m. It is thus possible that export flux at the base of the euphotic zone was very high on this cycle and that abnormally high flux attenuation was responsible for the moderate flux measured at 100 m. Whether this flux attenuation could be linked to the euphausiid swarms and their potential disruption of fecal pellets and marine snow during rapid swimming is a matter of speculation.

Restricting ourselves only to the measurements that we have made consistently at 100 m depth on all cruises, it is interesting that the regressions (on non-log transformed data) for the relationships between export-primary productivity and export-grazing both show a positive y-intercept of ~ 30 mg C m^{-2} d^{-1} (Fig. 6). This suggests that in the

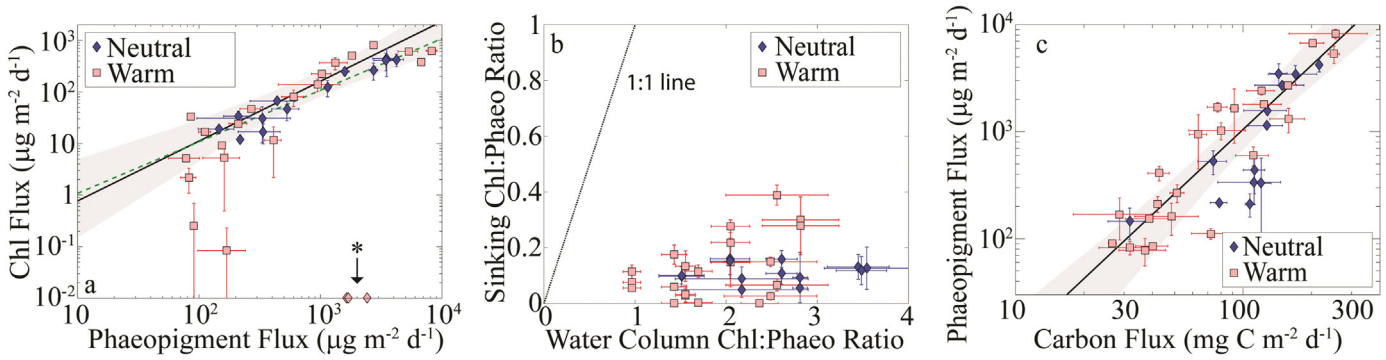

Fig. 7. Pigment flux measured in sediment traps. a) Chl *a* flux plotted against phaeopigment flux. Solid gray line depicts a constant Chl:Phaeo ratio of 0.11 (median of ratios for all samples). Dashed black line is Type II regression: $\log_{10}(\text{Chl}) = 1.16 \times \log_{10}(\text{Phaeo}) - 1.27$. *All tubes from P1604-3 measured no Chl, but substantial Phaeo. They were excluded from the regression. b) Ratio of vertically integrated Chl *a* to vertically integrated Phaeo in the euphotic zone (x-axis) and ratio of Chl *a* to Phaeo in sinking material. Dotted line is 1:1 line. Note that sinking material was substantially enriched in Phaeo relative to suspended material in the water column. c) Phaeopigment flux plotted against particulate organic carbon flux. Type II regression line is: $\log_{10}(\text{Phaeo}) = 2.0 \times \log_{10}(\text{Carbon}) - 0.96$. In all panels, units of phaeophigment flux are µg Chl *a* equivalent m^{-2} d^{-1}.

absence of contemporaneous primary productivity or grazing, we should expect continued measurable POC export. A regression of Phaeo flux against carbon flux suggested that at a similar export rate (specifically, 27 mg C m^{-2} d^{-1}) we should expect no contribution of phaeopigments (or Chl *a*) in the sediment traps. Taken together, this evidence suggests that sinking flux in the CCE is likely comprised of two distinct particle classes: 1) one component that contributes a relatively constant ~ 30 mg C m^{-2} d^{-1} to carbon flux and is likely comprised of slowly sinking particles with no measurable pigment content, and 2) another component that includes particles recently generated by processes in the overlying water column and is comprised primarily of fecal pellets. This possible dichotomy simultaneously explains the dominance of Phaeo over Chl in the sediment traps, the increasing relative contribution of Phaeo when carbon flux is high, and the concave-downward shape of functional relationships between carbon export and either primary production or mesozooplankton grazing. Nevertheless, there are likely other processes affecting carbon export in the CCE that have not been addressed in this study, including mineral ballasting of sinking material by Si-dense, Fe-stressed diatoms (Brzezinski et al., 2015), potential non-linear dynamics in frontal regions (Krause et al.,

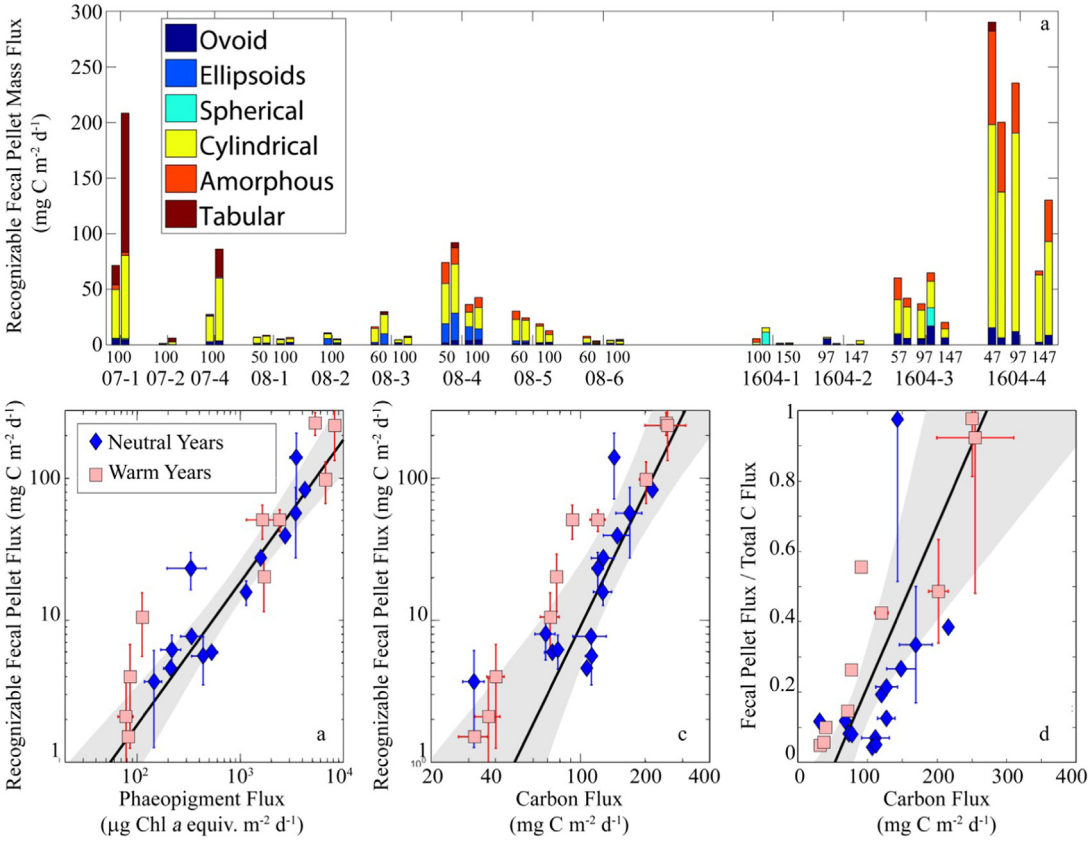

Fig. 8. Flux of recognizable fecal pellets into sediment traps. a) Pellet flux for each Lagrangian cycle and depth categorized by pellet shape (typically two replicates per cycle and depth). b) Fecal pellet flux plotted against Phaeo flux. Type II linear regression is: $\log_{10}(\text{FP Flux}) = 1.0 \times \log_{10}(\text{Phaeo Flux}) - 1.7$. c) Fecal pellet flux plotted against carbon flux. Type II linear regression is: $\log_{10}(\text{FP Flux}) = 3.1 \times \log_{10}(\text{C Flux}) - 5.3$. d) The relative contribution of fecal pellets to total carbon flux plotted against total carbon flux. Type II linear regression is: $\text{FP/Total} = 4.6 \times 10^{-3} \times \text{C Flux} - 0.25$.

2015; Stukel et al., 2017), and lateral advection of particles from the upwelling region to the oligotrophic region (Kelly et al., in this issue; Plattner et al., 2005).

5. Conclusions

We assessed the constancy of functional relationships (i.e., photosynthesis vs. irradiance, mesozooplankton grazing vs. chlorophyll, export fluxes vs. primary production or mesozooplankton grazing, carbon fluxes vs. fecal pellet fluxes or pigment fluxes) between neutral conditions in the California Current Ecosystem and the warm conditions of 2014–2016 (Warm Anomaly and El Niño). Overall, results showed strong similarities between years, with relatively few changes in the functional relationships between key variables controlling the biological carbon pump. When productivity was high, export was driven by the production and sinking of mesozooplankton fecal pellets as evidenced by the prevalence of recognizable fecal pellets in microscopically-sorted material and the dominance of phaeopigments relative to Chl. However, in oligotrophic regions export was dominated by material whose source could not be identified microscopically or by pigments. Instead, it seems likely that there is a background flux of slowly-sinking, degraded particles that dominates the signal in offshore regions in both warm and neutral years. We similarly found no significant differences in the response of mesozooplankton grazing to Chl concentrations in neutral and warm conditions, although it is possible that high variability in grazing rates may mask the importance of compositional shifts between years. In contrast to export and grazing, primary productivity was depressed during warm years relative to neutral years at similar nutrient concentrations. Whether this resulted from a shift toward subtropical species that were advected into the region as a result of the warm anomaly in 2014 and ensuing El Niño, or simply reflects selection for fast-growing species when upwelling is high during neutral years, deserves further attention.

Acknowledgments

We gratefully thank many colleagues in the CCE LTER program who contributed substantially to our seagoing program and to analyses conducted in the laboratory. We especially acknowledge M. Landry who contributed greatly to investigation of the zooplankton-export relationships and was integral to the design of our field campaigns. We also thank the captains and crews of the R/V Melville, R/V Knorr, R/V Thompson, and R/V Sikuliaq. All data used in this manuscript can be found on the CCE LTER Datazoo website (http://oceaninformatics.ucsd.edu/datazoo/catalogs/ccelter/datasets). This work was funded by NSF Bio Oce grants to the CCE LTER Program: OCE-0417616, OCE-1637632, and OCE-1614359.

References

Alexander, M.A., Bladé, I., Newman, M., Lanzante, J.R., Lau, N.-C., Scott, J.D., 2002. The atmospheric bridge: the influence of ENSO teleconnections on air–sea interaction over the global oceans. J. Clim. 15 (16), 2205–2231.

Auth, T.D., Daly, E.A., Brodeur, R.D., Fisher, J.L., 2017. Phenological and distributional shifts in ichthyoplankton associated with recent warming in the northeast Pacific Ocean. Glob. Change Biol.

Bamstedt, U., Gifford, D.J., Irigoien, X., Atkinson, A., Roman, M., 2000. Feeding. In: Harris, R.P., Wiebe, P.H., Lenz, J., Skjodal, H.R., Huntley, M. (Eds.), ICES Zooplankton Methodology Manual. Academic Press, London, pp. 297–399.

Benitez-Nelson, C.R., Buesseler, K.O., van der Loeff, M.R., Andrews, J., Ball, L., Crossin, G., Charette, M.A., 2001. Testing a new small-volume technique for determining Th-234 in seawater. J. Radioanal. Nucl. Chem. 248 (3), 795–799.

Bograd, S.J., Lynn, R.J., 2001. Physical-biological coupling in the California Current during the 1997–99 El Niño-La Niña Cycle. Geophys. Res. Lett. 28 (2), 275–278.

Bond, N.A., Cronin, M.F., Freeland, H., Mantua, N., 2015. Causes and impacts of the 2014 warm anomaly in the NE Pacific. Geophys. Res. Lett. 42 (9), 3414–3420.

Brzezinski, M.A., Krause, J.W., Bundy, R.M., Barbeau, K.A., Franks, P., Goericke, R., Landry, M.R., Stukel, M.R., 2015. Enhanced silica ballasting from iron stress sustains carbon export in a frontal zone within the California Current. J. Geophys. Res.: Oceans 120 (7), 4654–4669.

Chavez, F., Pennington, J., Castro, C., Ryan, J., Michisaki, R., Schlining, B., Walz, P., Buck, K., McFadyen, A., Collins, C., 2002. Biological and chemical consequences of the 1997–1998 El Niño in central California waters. Prog. Oceanogr. 54 (1), 205–232.

Chelton, D.B., Bernal, P., McGowan, J.A., 1982. Large-scale interannual physical and biological interaction in the California Current. J. Mar. Res. 40 (4), 1095–1125.

Clarke, A.J., Dottori, M., 2008. Planetary wave propagation off California and its effect on zooplankton. J. Phys. Oceanogr. 38 (3), 702–714.

Dam, H.G., Peterson, W.T., 1988. The effect of temperature on the gut clearance rate-constant of planktonic copepods. J. Exp. Mar. Biol. Ecol. 123 (1), 1–14.

Di Lorenzo, E., Mantua, N., 2016. Multi-year persistence of the 2014/15 North Pacific marine heatwave. Nat. Clim. Change 6 (11), 1042–1047.

Downs, J.N., Lorenzen, C.J., 1985. Carbon: pheopigment ratios of zooplankton fecal pellets as an index of herbivorous feeding. Limnol. Oceanogr. 30 (5), 1024–1036.

Ducklow, H.W., Steinberg, D.K., Buesseler, K.O., 2001. Upper ocean carbon export and the biological pump. Oceanography 14 (4), 50–58.

Dunne, J.P., Armstrong, R.A., Gnanadesikan, A., Sarmiento, J.L., 2005. Empirical and mechanistic models for the particle export ratio. Glob. Biogeochem. Cycles 19 (4), GB4026.

Fisher, J.L., Peterson, W.T., Rykaczewski, R.R., 2015. The impact of El Niño events on the pelagic food chain in the northern California Current. Glob. Change Biol. 21 (12), 4401–4414.

Frischknecht, M., Münnich, M., Gruber, N., 2015. Remote versus local influence of ENSO on the California Current System. J. Geophys. Res.: Oceans 120 (2), 1353–1374.

Frischknecht, M., Münnich, M., Gruber, N., 2017. Local atmospheric forcing driving an unexpected California Current System response during the 2015–2016 El Niño. Geophys. Res. Lett. 44 (1), 304–311.

Gentemann, C.L., Fewings, M.R., García-Reyes, M., 2017. Satellite sea surface temperatures along the West Coast of the United States during the 2014–2016 northeast Pacific marine heat wave. Geophys. Res. Lett. 44 (1), 312–319.

Goericke, R., Ohman, M.D., 2015. Introduction to CCE-LTER: responses of the California Current Ecosystem to climate forcing. Deep Sea Res. Part II: Top. Stud. Oceanogr. 112, 1–5.

Gómez-Ocampo, E., Durazo, R., Gaxiola-Castro, G., De la Cruz-Orozco, M., Sosa-Ávalos, R., 2017. Effects of the interannual variability of water column stratification on phytoplankton production and biomass in the northern zone off Baja California. Cienc. Mar. 43, 2.

Henson, S.A., Sanders, R., Madsen, E., Morris, P.J., Le Moigne, F., Quartly, G.D., 2011. A reduced estimate of the strength of the ocean's biological carbon pump. Geophys. Res. Lett. 38.

Jackson, G.A., Checkley, D.M., 2011. Particle size distributions in the upper 100 m water column and their implications for animal feeding in the plankton. Deep-Sea Res. I 58 (3), 283–297.

Jacox, M.G., Hazen, E.L., Zaba, K.D., Rudnick, D.L., Edwards, C.A., Moore, A.M., Bograd, S.J., 2016. Impacts of the 2015–2016 El Niño on the California Current System: early assessment and comparison to past events. Geophys. Res. Lett. 43 (13), 7072–7080.

Kahru, M., Jacox, M.G., Ohman, M.D. CCE I: The effect of the2014-2016 northeast Pacific warm anomalies on the frequency of oceanic fronts and surface chlorophyll concentration in the California Current System. Deep-Sea Res. I (in this issue).

Kahru, M., Lee, Z., Kudela, R.M., Manzano-Sarabia, M., Greg Mitchell, B., 2015. Multi-satellite time series of inherent optical properties in the California Current. Deep Sea Res. II 112, 91–106.

Kahru, M., Mitchell, B.G., 2000. Influence of the 1997-98 El Niño on the surface chlorophyll in the California Current. Geophys. Res. Lett. 27 (18), 2937–2940.

Kahru, M., Mitchell, B.G., 2002. Influence of the El Niño-La Niña cycle on satellite-derived primary production in the California Current. Geophys. Res. Lett. 29 (17), 4.

Kelly, T.B., Goericke, R., Kahru, M., Song, H., Stukel, M.R.. CCE II: Spatial and interannual variability in export efficiency and the biological pump in an eastern boundary current upwelling system with substantial lateral advection. Deep-Sea Res. I. (in this issue).

Knauer, G.A., Martin, J.H., Bruland, K.W., 1979. Fluxes of particulate carbon, nitrogen, and phosphorus in the upper water column of the Northeast Pacific. Deep-Sea Res. 26 (1), 97–108.

Krause, J.W., Brzezinski, M.A., Goericke, R., Landry, M.R., Ohman, M.D., Stukel, M.R., Taylor, A.G., 2015. Variability in diatom contributions to biomass, organic matter production and export across a frontal gradient in the California Current Ecosystem. J. Geophys. Res. Oceans 120 (2), 1032–1047.

Landry, M.R., Ohman, M.D., Goericke, R., Stukel, M.R., Barbeau, K.A., Bundy, R., Kahru, M., 2012. Pelagic community responses to a deep-water front in the California Current Ecosystem: overview of the A-front study. J. Plankton Res. 34 (9), 739–748.

Landry, M.R., Ohman, M.D., Goericke, R., Stukel, M.R., Tsyrklevich, K., 2009. Lagrangian studies of phytoplankton growth and grazing relationships in a coastal upwelling ecosystem off Southern California. Prog. Oceanogr. 83, 208–216.

Lavaniegos, B.E., Ohman, M.D., 2007. Coherence of long-term variations of zooplankton in two sectors of the California Current System. Prog. Oceanogr. 75 (1), 42–69.

Laws, E.A., D'Sa, E., Naik, P., 2011. Simple equations to estimate ratios of new or export production to total production from satellite-derived estimates of sea surface temperature and primary production. Limnol. Oceanogr.-Methods 9, 593–601.

Li, Q.P., Franks, P.J.S., Landry, M.R., Goericke, R., Taylor, A.G., 2010. Modeling phytoplankton growth rates and chlorophyll to carbon ratios in California coastal and pelagic ecosystems. J. Geophys. Res.-Biogeosci. 115, G04003.

Lilly, L.E., Ohman, M.D.. CCE IV: El Niño-related zooplankton variability in the southern California Current System. Deep-Sea Res. I. (in this issue).

Linacre, L., Lara-Lara, J.R., Mirabal-Gómez, U., Durazo, R., Bazán-Guzmán, C., 2017. Microzooplankton grazing impact on the phytoplankton community at a coastal upwelling station off northern Baja California, Mexico. Cienc. Mar. 43, 2.

McCabe, R.M., Hickey, B.M., Kudela, R.M., Lefebvre, K.A., Adams, N.G., Bill, B.D.,

Gulland, F., Thomson, R.E., Cochlan, W.P., Trainer, V.L., 2016. An unprecedented coastwide toxic algal bloom linked to anomalous ocean conditions. Geophys. Res. Lett. 43, 19.

McClatchie, S., Goericke, R., Leising, A., Auth, T., Bjorkstedt, E., Roberson, R.R., Brodeur, R.D., Du, X., Daly, E.A., Morgan, C.A., Chavez, F.P., Debich, A.J., Hildebrand, J., Field, J., Sakuma, K., Jacox, M., Kahru, M., Kudela, R., Anderson, C., Lavaniegos, B.E., Gomez-Valdes, J., Jimenez-Rosenberg, S.P.A., McCabe, R., Melin, S., Ohman, M.D., Sala, L.M., Peterson, B., Fisher, J., Schroeder, I.D., Bograd, S.J., Hazen, E.L., Schneider, S.R., Golightly, R.T., Suryan, R.M., Gladics, A.J., Loredo, S., Porquez, J.M., Thompson, A.R., Weber, E.D., Watson, W., Trainer, V., Warzybok, P., Bradley, R., Jahncke, M., 2016. State of the California Current 2015–16: comparisons with the 1997–98 El Niño. California cooperative oceanic fisheries investigations. Data Rep. 57, 1–57.

McKibben, S.M., Peterson, W., Wood, A.M., Trainer, V.L., Hunter, M., White, A.E., 2017. Climatic regulation of the neurotoxin domoic acid. Proc. Natl. Acad. Sci. USA 114 (2), 239–244.

Michaels, A.F., Silver, M.W., 1988. Primary production, sinking fluxes and the microbial food web. Deep-Sea Res. 35 (4), 473–490.

Nickels, C.F., Ohman, M.D., 2018. CCEIII: Persistent functional relationships between copepod egg production rates and food concentration through anomalously warm conditions in the California Current Ecosystem. Deep. Sea. Res. https://doi.org/10.1016/j.dsr.2018.07.001.

Ohman, M.D., Barbeau, K., Franks, P.J.S., Goericke, R., Landry, M.R., Miller, A.J., 2013. Ecological transitions in a coastal upwelling ecosystem. Oceanography 26 (3), 210–219.

Ohman, M.D., Mantua, N., Keister, J., Garcia-Reyes, M., MCClatchie, S., 2017. ENSO impacts on ecosystem indicators in the California Current system. US Clivar Var. 15 (1), 8–15.

Ohman, M.D., Powell, J.R., Picheral, M., Jensen, D.W., 2012. Mesozooplankton and particulate matter responses to a deep-water frontal system in the southern California Current System. J. Plankton Res. 34 (9), 815–827.

Owens, S.A., Buesseler, K.O., Sims, K.W.W., 2011. Re-evaluating the ^{238}U-salinity relationship in seawater: implications for the ^{238}U-^{234}Th disequilibrium method. Mar. Chem. 127 (1–4), 31–39.

Peterson, W.T., Fisher, J.L., Strub, P.T., Du, X., Risien, C., Peterson, J., Shaw, C.T., 2017. The pelagic ecosystem in the Northern California Current off Oregon during the 2014–2016 warm anomalies within the context of the past 20 years. J. Geophys. Res.: Oceans 122 (9), 7267–7290.

Pike, S.M., Buesseler, K.O., Andrews, J., Savoye, N., 2005. Quantification of ^{234}Th recovery in small volume sea water samples by inductively coupled plasma-mass spectrometry. J. Radioanal. Nucl. Chem. 263 (2), 355–360.

Plattner, G.K., Gruber, N., Frenzel, H., McWilliams, J.C., 2005. Decoupling marine export production from new production. Geophys. Res. Lett. https://doi.org/10.1029/2005GL022660.

Rebstock, G.A., 2001. Long-term stability of species composition in calanoid copepods off southern California. Mar. Ecol. Prog. Ser. 215, 213–224.

Rebstock, G.A., 2003. Long-term change and stability in the California Current System: lessons from CalCOFI and other long-term data sets. Deep-Sea Res. Part II-Top. Stud. Oceanogr. 50 (14–16), 2583–2594.

Rudnick, D.L., Zaba, K.D., Todd, R.E., Davis, R.E., 2017. A climatology of the California Current system from a network of underwater gliders. Prog. Oceanogr. 154 (Suppl. C), S64–S106.

Sánchez-Velasco, L., Beier, E., Godínez, V.M., Barton, E.D., Santamaría-del-Angel, E., Jiménez-Rosemberg, S.P.A., Marinone, S.G., 2017. Hydrographic and fish larvae distribution during the "Godzilla El Niño 2015–2016" in the northern end of the shallow oxygen minimum zone of the Eastern Tropical Pacific Ocean. J. Geophys. Res.: Oceans 122 (3), 2156–2170.

Shipe, R.F., Passow, U., Brzezinski, M.A., Graham, W.M., Pak, D.K., Siegel, D.A., Alldredge, A.L., 2002. Effects of the 1997-98 El Niño on seasonal variations in suspended and sinking particles in the Santa Barbara basin. Prog. Oceanogr. 54 (1–4), 105–127.

Siegel, D.A., Buesseler, K.O., Doney, S.C., Sailley, S.F., Behrenfeld, M.J., Boyd, P.W., 2014. Global assessment of ocean carbon export by combining satellite obervations and food-web models. Glob. Biogeochem. Cycles 28 (3), 181–196.

Silverberg, N., Martinez, A., Aguiniga, S., Carriquiry, J.D., Romero, N., Shumilin, E., Cota, S., 2004. Contrasts in sedimentation flux below the southern California Current in late 1996 and during the El Nino event of 1997–1998. Estuar. Coast. Shelf Sci. 59 (4), 575–587.

Smith, K.L., Baldwin, R.J., Ruhl, H.A., Kahru, M., Mitchell, B.G., 2006. Climate effect on food supply to depths greater than 4,000 m in the northeast Pacific. Limnol. Oceanogr. 51 (1), 166–176.

Steinberg, D.K., Landry, M.R., 2017. Zooplankton and the ocean carbon cycle. Annu. Rev. Mar. Sci. 9, 413–444.

Strickland, J.D., Parsons, T.R., 1972. A Practical Handbook of Seawater Analysis, second. Bulletin of the Fisheries Research Board of Canada, Ottawa, Canada.

Stukel, M.R., Aluwihare, L.I., Barbeau, K.A., Chekalyuk, A.M., Goericke, R., Miller, A.J., Ohman, M.D., Ruacho, A., Song, H., Stephens, B.M., Landry, M.R., 2017. Mesoscale ocean fronts enhance carbon export due to gravitational sinking and subduction. Proc. Natl. Acad. Sci. USA.

Stukel, M.R., Kahru, M., Benitez-Nelson, C.R., Decima, M., Goericke, R., Landry, M.R., Ohman, M.D., 2015. Using Lagrangian-based process studies to test satellite algorithms of vertical carbon flux in the eastern North Pacific Ocean. J. Geophys. Res.: Oceans 120, 7208–7222.

Stukel, M.R., Landry, M.R., Benitez-Nelson, C.R., Goericke, R., 2011. Trophic cycling and carbon export relationships in the California Current Ecosystem. Limnol. Oceanogr. 56 (5), 1866–1878.

Stukel, M.R., Landry, M.R., Ohman, M.D., Goericke, R., Samo, T., Benitez-Nelson, C.R., 2012. Do inverse ecosystem models accurately reconstruct plankton trophic flows? Comparing two solution methods using field data from the California Current. J. Mar. Syst. 91 (1), 20–33.

Stukel, M.R., Ohman, M.D., Benitez-Nelson, C.R., Landry, M.R., 2013. Contributions of mesozooplankton to vertical carbon export in a coastal upwelling system. Mar. Ecol. Prog. Ser. 491, 47–65.

Turner, J.T., 2015. Zooplankton fecal pellets, marine snow, phytodetritus and the ocean's biological pump. Prog. Oceanogr. 130 (0), 205–248.

Venrick, E.L., 2002. Floral patterns in the California Current System off southern California: 1990–1996. J. Mar. Res. 60 (1), 171–189.

Wang, S.Y., Hipps, L., Gillies, R.R., Yoon, J.H., 2014. Probable causes of the abnormal ridge accompanying the 2013–2014 California drought: ENSO precursor and anthropogenic warming footprint. Geophys. Res. Lett. 41 (9), 3220–3226.

Welschmeyer, N.A., 1994. Fluorometric analysis of chlorophyll a in the presence of chlorophyll b and pheopigments. Limnol. Oceanogr. 39 (8), 1985–1992.

Wilson, S.E., Steinberg, D.K., Buesseler, K.O., 2008. Changes in fecal pellet characteristics with depth as indicators of zooplankton repackaging of particles in the mesopelagic zone of the subtropical and subarctic North Pacific Ocean. Deep-Sea Res. II 55 (14–15), 1636–1647.

York, D., Evensen, N.M., Martinez, M.L., Delgado, J.D., 2004. Unified equations for the slope, intercept, and standard errors of the best straight line. Am. J. Phys. 72 (3), 367–375.

Zaba, K.D., Rudnick, D.L., 2016. The 2014–2015 warming anomaly in the Southern California Current System observed by underwater gliders. Geophys. Res. Lett. 43 (3), 1241–1248.